

Contents lists available at ScienceDirect

# Case Studies in Thermal Engineering

journal homepage: www.elsevier.com/locate/csite



# Thermal dynamics of nanoparticle aggregation in MHD dissipative nanofluid flow within a wavy channel: Entropy generation minimization



Muhammad Idrees Afridi <sup>a</sup>, Abid Hussanan <sup>b</sup>, Muhammad Qasim <sup>c,\*</sup>, Ali J. Chamkha <sup>d</sup>

- <sup>a</sup> School of Mathematics and Computer Science, Hanjiang Normal University, Shiyan, 442000, China
- <sup>b</sup> Department of Mathematics, Division of Science and Technology, University of Education, Lahore, Pakistan
- <sup>c</sup> Department of Mathematics, COMSATS University Islamabad (CUI), Park Road, Tarlai Kalan, Islamabad, 45550, Pakistan
- <sup>d</sup> Faculty of Engineering, Kuwait College of Science and Technology, Doha District, 35004, Kuwait

### ARTICLE INFO

### Keywords:

Nanoparticles aggregation Viscous dissipation Heat transfer Entropy generation Numerical simulation Joule heating

### ABSTRACT

This paper examines how nanoparticle aggregation and a consistent magnetic field influence the peristaltic movement of a dissipative nanofluid, which is caused by the sinusoidal deformation of the boundary. The viscosity of TiO2/H2O nanofluids is accurately determined by the Krieger-Dougherty model with nanoparticle aggregation, while thermal conductivity (TC) is estimated through the Bruggeman model. The set of governing equations are modeled in a fixed frame by utilizing the conservation laws of energy, mass and momentum. Galilean transformation is utilized to transform the system of equations into a wave frame, which is then converted into a dimensionless form. The assumption of a small Reynolds number and long wavelength serve to further simplify the set of equations, which are subsequently addressed through the implementation of the differential quadrature method (DQM), a highly effective numerical technique. Quantities of interest, namely velocity, pressure gradient, temperature, trapping phenomena, heat transfer, and volumetric entropy generation are analyzed across a range of physical parameters, including the solid volume fraction ( $\Phi = 0.01 - 0.04$ ), Eckert number (Ec = 0.0 - 0.1), Hartman number  $(M_h = 0.2 - 2.2)$ , Grashof number (Gr = 1.0 - 3.0) and temperature ratio parameter  $(\theta_d = 0.5 - 2.5)$ . A comparative analysis is conducted between the scenario involving aggregation and the one without aggregation. It is observed that nanoparticle aggregation significantly alters these quantities.

# Nomenclature

Symbol Name

 $a_1, a_2$  Waves amplitudes  $B_0$  Magnetic field intensity

c Speed of wave

 $c_p$  Specific heat capacity

E-mail address: mq\_qau@yahoo.com (M. Qasim).

# https://doi.org/10.1016/j.csite.2024.105054

<sup>\*</sup> Corresponding author.

The Eckert number Ес F Non-dimensional flow rate (wave frame) Gr Grashof number  $H_1^*, H_2^*$ Right and Left walls Thermal conductivity Ns Entropy generation number Magnetic parameter  $M_h$  $P^*, \overline{P}$ Pressure fields in laboratory and wave frame Pr Prandtl number Re Revnolds number  $\dot{S}_{gen}^{'''}$ Volumetric Entropy generation rate Characteristic entropy Dimensional temperature fields  $U^*.V^*$ Unit less velocity components (laboratory frame)  $\overline{U}$ ,  $\overline{V}$ Unit less velocity components (wave frame)  $X^*.Y^*$ Rectangular space coordinates (laboratory frame)  $\overline{X}, \overline{Y}$ Rectangular space coordinates (wave frame) Volume fraction of nanoparticles Θ Dimensionless Temperature β Thermal expansion coefficient σ Electrical conductivity Dimensionless flow rate (laboratory frame) χ Dynamic viscosity μ Density ρ λ Wavelength Phase difference Φ Temperature difference parameter  $\theta_d$ Unit less stream function W Nanofluid nf bf Base fluid

# 1. Introduction

It is now well-established that suspending solid particles in conventional fluids can significantly enhance their thermophysical properties, including viscosity, density, electrical conductivity, and thermal conductivity. The dispersal of nanoparticles with dimensions smaller than 100 nm within conventional fluids is referred to as "nanofluid", a nomenclature introduced by Choi [1], who first experimentally uncovered this phenomenon. Mishra et al. [2] conducted a literature review, affirming that nanofluid viscosity is influenced by various factors, including base fluids (ordinary fluids like water), particles solid volume fraction, shape, size, temperature, aggregation, shear rate, surfactants, pH, and dispersion methods. Angayarkanni and Philip [3] undertook an extensive examination of the literature concerning nanofluids, addressing various aspects including stability requirements, preparation methodologies, and approaches for quantifying thermal conductivity. Moreover, they mentioned a range of experimental findings to elucidate the thermal characteristics of nanofluids. The flow of nanofluids holds significant importance across diverse domains, encompassing biomedical sciences (e.g., drug delivery and diagnostics) and engineering applications (e.g., enhancing heat transfer and lubrication). In automotive engineering, nanofluids play a vital role in augmenting engine cooling systems and effectively dissipating heat from electronic components. This advancement contributes to enhancing overall vehicle performance and reliability, as documented in Refs. [4–12].

Peristaltic transport in sinusoidal wavy channels has gained significance in physiology, biomedical engineering, and various industries. Ongoing research focuses on peristaltic flow, particularly in medical devices and artificial organs such as dialysis machines and artificial hearts. Accurate regulation of fluid movement is crucial for peristaltic pumps used in drug delivery systems to ensure precise dosing for patients. Additionally, peristaltic pumping finds applications in the food and beverage, wastewater treatment, and chemical processing industries, offering advantages in preventing fluid contamination or damage due to the contained nature of the fluid within the tube, away from the pump mechanism. Foundational theoretical and experimental work on this subject has been accomplished by a group of scholars, including Latham [13], Burns and Parkes [14], Fung and Yi [15], Zein and Ostrach [16], Shapiro et al. [17], Srivastava and Srivastava [18], Brown and Hung [19]. Peristalsis combined with heat transfer finds application in various fields such as thermal therapy techniques, controlled heating or cooling of fluids during peristaltic pumping, and in food processing industries for cooking, pasteurization, and sterilization processes. Additionally, it is relevant in chemical engineering processes like mixing and separation. The peristaltic flow of nanofluids, particularly when subjected to a magnetic field, demonstrates a diverse array of uses in multiple scientific and engineering disciplines for examples lab-on-a-chip devices, hyperthermia therapy,

magnetohydrodynamic (MHD) pumps and generators, magnetic resonance imaging, drug delivery, ultrasound imaging, and more. Akbar's [20] examined a peristaltic mechanism of copper/water nanofluid within a tube of uniform diameter subjected to a magnetic field, while also examining the heat transfer phenomena linked with it. Noreen et al. [21] studied mixed convection in the peristaltic motion of blood flow containing copper nanoparticles. Sara and Bhatti [22] documented a report on the influence of a fluctuating magnetic force on the Prandtl nanofluid (a mixture of blood and TiO<sub>2</sub>) in an endoscope. Prakash et al. [23] conducted a relative analysis of electro-osmotically intensified peristaltic flow of nanofluids considering water as working fluid, incorporating metallic nanoparticles like titania, alumina, and copper. The effect of strong magnetic field over the flow of a copper-water nanofluid within an asymmetric channel, considering ion slip and Hall current, was reported by Das et al. [24]. The equations are modified through small Reynolds number approximations along with long wavelength assumptions, to yield a closed-form exact solution. A comparative study between single particle nanofluid (Cu-water) and hybrid nanofluid (SiO<sub>2</sub>-copper-water) transport in a wavy tube is presented by Iftikhar et al. [25]. They also conducted a comparison between nanoparticles of different shapes. Models of nanofluids used in this study are based on the experiments almost similar to Das and Barman [24] who analyzed ionic hybrid metallic/oxide nanoparticles behavior through electro-osmotic flow/peristaltic within a porous-vertical microchannel. Ion-slip along with Hall currents were also included in their discussions, as the equations of motion admitted exact solutions under dimensionless form upon application of Debye-Hückel linearization together with large wavelength/small Reynolds number assumptions. Ashraf et al. [27] analyzed the peristaltic transport of blood infused with cylindrical gold nanoparticles within a non-uniformly shaped conduit. In their simulation, Das et al. [28] took into account magnetic fields, Hall currents, ion-slip currents, wall slip, and convective heating while simulating electroosmosis-modulated peristaltic flow of a Casson-model ionic hybrid nano-fluid (silicon and silver dioxide nanoparticles in water) through a microchannel integrated with porous medium. The electro-osmotic peristalsis of a ternary hybrid nanofluid (blood and gold-copper-titania) within diverging-converging ciliated microchannel was scrutinized by Ali et al. [29].

Waheed et al. [30] documented a study on the peristaltic movement of a ternary-hybrid nanofluid containing alumina, silver, and copper nanoparticles that are distributed in water. The peristaltic flow of hybrid nanofluid blood through a micro-vessel was documented by Ali et al. [31], by considering Lorentz force and a heat source. They simplified the equations using Debye-Hückel linearization and lubrication theory, and applied the analytical method to get the series solutions for the non-dimensional equations. In engineering, heat transfer must maintain energy quality and mitigate degradation throughout the heat transfer process. The first principle of thermodynamics ensures that total energy remains constant, while the second law indicates a consistent decline in energy quality, as measured by entropy. The goal is to minimize entropy generation to preserve energy quality in fluid flow problems. Understanding the entropy production in the flow volume is crucial for this objective. Minimizing entropy generation significantly enhances system performance [32-41]. Akbar et al. [42] conducted a second law analysis within the peristaltic motion of a nanofluid containing copper nanoparticles and water. In a comparable investigation, Qasim et al. [43] examined the entropy production within the motion of a nanofluid, where methanol served as the base fluid, passing through a channel that exhibited asymmetrical deformability. Akbar and Butt [44] have delineated the origins of entropy production during the peristaltic flow of nanofluid through a uniformly wavy tube. Noreen et al. [44] analyzed electroosmotic flow of water-based nanofluid in an asymmetric porous channel. Entropy generation analysis is also conducted is the presence of viscous heating. Using hybrid Cu-Ag nanoparticles in a heat-sourced tube, Ali et al. [46] examined entropy formation and heat transmission in ciliary-induced peristaltic blood flow. This analysis employed the Phan-Thien-Tanner model to elucidate the blood's non-Newtonian behavior.

All studies [20–46] on the peristaltic flow of various types of nanofluids were conducted without taking nanoparticle aggregation. The aggregating changes the surface area and effective dimensions of the nanoparticles, therefore affecting the thermal conductivity and viscosity of the nanofluid The phenomenon of aggregation has the capability to significantly influence the efficiency and resilience of nanofluids across a wide range of uses, including, such as thermal management, biomedical imaging, and drug delivery. Therefore, controlling the aggregating of nanoparticles is important and the proper distribution of nanoparticles could lead to improved nanofluid characteristics and performance [47–51]. Therefore, this article aims to examine the influence of nanoparticle aggregation on the peristaltic transport of a dissipative TiO<sub>2</sub>/H<sub>2</sub>O nanofluid in a vertical asymmetric channel. Additionally, the study includes an analysis of entropy to quantify irreversibilities and thermodynamic effectiveness. This improved our understanding of the ways in which fluid friction, magnetic field, solid volume fraction, and nanoparticle aggregation affect the system's performance. This article is structured in the following manner: Section two, presents mathematical modeling following the introduction. In addition to modeling the governing equations through conservation laws, the thermophysical characteristics of the nanofluid are also explained in detail. Section three provides the expression for the volumetric production rate in both fixed and wave frames, and its conversion to dimensionless form. Section four details the numerical scheme. Section five, offers a graphical analysis of physical quantities versus various parameters. Finally, significant observations are included in Section 6.

### 2. The mathematical model

Before introducing the mathematical model, the subsequent assumptions are taken into account.

- 1. Nanofluid is Newtonian and incompressible.
- 2. The flow of the fluid is laminar, fully developed, steady and two-dimensional.
- 3. The magnetic field is uniformly applied normally to the flow of the channel.
- 4. The channel is vertical.
- 5. The effect of the gravity and the pressure gradient are considered.
- 6. The induced magmatic field is not considered.

We examine the mixed convection behavior of a dissipative nanofluid in a flexible, asymmetrical vertical channel with wavy walls, focusing on the influence of nanoparticles (NPs) aggregation (agg.), viscous dissipation, and magnetic heating. The rectangular coordinates system  $(X^*, Y^*)$  is defined in a manner that the length of the channel is alinged with  $X^*$  – axis and width of the channel  $w_1 + w_2$  is along the  $Y^*$  – axis (see Fig. 1). The movement of nanofluid inside the wavy channel is induced by a sinusoidal wave transmitting with velocity c along the deformable walls of the channel. The wavelength of the propagating waves along the channel is supposed to be  $\lambda$  whereas, the amplitudes at the right and left wall are supposed to be  $a_1$  and  $a_2$  respectively.

The geometry of the flexible boundaries of the channel are formally described through mathematical expressions as [24].

$$\begin{cases} & \mathsf{Y}^* = H_1^*(X^*,t^*) = w_1 + \cos\left(\frac{2\pi}{\lambda}(X^* - ct^*)\right)a_1, & \text{Right Wall} \\ & \\ Y^* = H_2^*(X^*,t^*) = -w_2 + \left(-\cos\left(\frac{2\pi}{\lambda}(X^* - ct^*) + \varphi\right)a_2\right) & \text{Left Wall} \end{cases}$$

Here  $\varphi$  shows the phase difference and  $t^*$  represents time. Further,  $w_1, w_2, a_1, a_2$  and  $\varphi$  satisfy  $a_1^2 + a_2^2 + 2a_1a_2 \cos \varphi \le (w_1 + w_2)^2$ . The rectangular components of velocity with respect to the stationary frame are  $U^*(X^*, Y^*, t^*)$  and  $V^*(X^*, Y^*, t^*)$ . The temperature of the right and left walls of the channel is supposed to be constant and respectively denoted by  $T_0$  and  $T_1$ . Further, the applied magnetic force  $\overrightarrow{B} = (0, B_0, 0)$  is oriented normal to  $X^*$  – axis. The set governing equations relative to the stationary frame are [21,22,30]

$$\frac{\partial U^*}{\partial X^*} + \frac{\partial V^*}{\partial Y^*} = 0, \tag{2}$$

$$\rho_{nf}\left(\frac{\partial U^*}{\partial t^*} + U^* \frac{\partial U^*}{\partial X^*} + V^* \frac{\partial U^*}{\partial Y^*}\right) = \begin{cases} -\frac{\partial P^*}{\partial X^*} + \mu_{nf}\left(\frac{\partial^2 U^*}{\partial Y^{*2}} + \frac{\partial^2 U^*}{\partial X^{*2}}\right) \\ +g(\rho \beta)_{nf}(T^* - T_o) - \sigma_{nf}B_o^2 U^* \end{cases}$$

$$(3)$$

$$\rho_{nf}\left(\frac{\partial V^*}{\partial t^*} + U^*\frac{\partial V^*}{\partial X^*} + V^*\frac{\partial V^*}{\partial Y^*}\right) = -\frac{\partial P^*}{\partial Y^*} + \mu_{nf}\left(\frac{\partial^2 V^*}{\partial Y^{*2}} + \frac{\partial^2 V^*}{\partial X^{*2}}\right)$$
(4)

$$\frac{\partial T^{*}}{\partial t^{*}} + V^{*} \frac{\partial T^{*}}{\partial Y^{*}} + \frac{\partial T^{*}}{\partial X^{*}} U^{*} = \begin{cases}
\frac{1}{\left(\rho c_{p}\right)_{nf}} k_{nf} \left(\frac{\partial^{2} T^{*}}{\partial Y^{*2}} + \frac{\partial^{2} T^{*}}{\partial X^{*2}}\right) + \frac{\sigma_{nf} B_{o}^{2}}{\left(\rho c_{p}\right)_{nf}} U^{*2} \\
+ \frac{\mu_{nf}}{\left(\rho c_{p}\right)_{nf}} \left(2 \left(\frac{\partial U^{*}}{\partial X^{*}}\right)^{2} + 2 \left(\frac{\partial V^{*}}{\partial Y^{*}}\right)^{2} + \left(\frac{\partial U^{*}}{\partial Y^{*}} + \frac{\partial V^{*}}{\partial X^{*}}\right)^{2}\right).
\end{cases} (5)$$

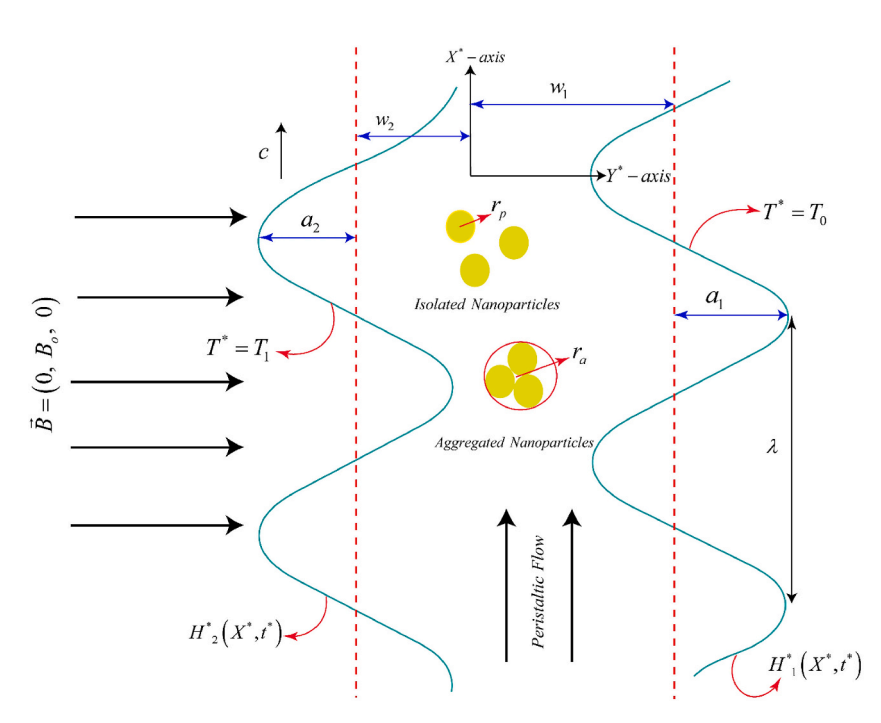


Fig. 1. Geometric depiction of the model for nanofluid flow.

The Galilean transformation equations [24] for time, space coordinates, and velocity components are

$$\left(\frac{\overline{X}}{\overline{Y}}\right) = \begin{pmatrix} X^* - ct \\ Y^* \end{pmatrix}, (\overline{t}) = (t^*), \begin{pmatrix} \overline{\overline{U}} \\ \overline{V} \end{pmatrix} = \begin{pmatrix} U^* - c \\ V^* \end{pmatrix}, \begin{pmatrix} \overline{P} \\ \overline{T} \end{pmatrix} = \begin{pmatrix} P^* \\ T^* \end{pmatrix}. \tag{6}$$

Here,  $(\overline{X}, \overline{Y})$  represents space coordinates relative to the inertial wave frame,  $(\overline{U}, \overline{V})$  shows the velocity components relative to the moving inertial frame,  $\overline{t}$  is the time in the moving inertial frame. Further  $\overline{t} = t^*$  because due to employment classical physics. In this context, time is regarded as an invariant entity; hence, the time observed in both stationary and moving frames (specifically, the wave frame) will exhibit identical characteristics. Using Eq. (6), Eqs. (2)–(5) take the following form:

$$\frac{\partial \overline{U}}{\partial \overline{X}} + \frac{\partial \overline{V}}{\partial \overline{Y}} = 0, \tag{7}$$

$$\rho_{nf}\left(\overline{U}\frac{\partial\overline{U}}{\partial\overline{X}} + \overline{V}\frac{\partial\overline{U}}{\partial\overline{Y}}\right) = \begin{cases}
-\frac{\partial\overline{P}}{\partial\overline{X}} + \mu_{nf}\left(\frac{\partial^{2}\overline{U}}{\partial\overline{Y}^{2}} + \frac{\partial^{2}\overline{U}}{\partial\overline{X}^{2}}\right) \\
+g(\rho\beta)_{nf}(\overline{T} - T_{0}) - \sigma_{nf}(T)B_{0}^{2}(\overline{U} + c),
\end{cases} (8)$$

$$\rho_{nf}\left(\overline{U}\frac{\partial \overline{V}}{\partial \overline{X}} + \overline{V}\frac{\partial \overline{V}}{\partial \overline{Y}}\right) = -\frac{\partial \overline{P}}{\partial \overline{Y}} + \mu_{nf}\left(\frac{\partial^2 \overline{V}}{\partial \overline{X}^2} + \frac{\partial^2 \overline{V}}{\partial \overline{V}^2}\right),\tag{9}$$

$$\overline{U}\frac{\partial \overline{T}}{\partial \overline{X}} + \overline{V}\frac{\partial \overline{T}}{\partial \overline{Y}} = \begin{cases}
\frac{\mu_{nf}}{(\rho c_p)_{nf}} \left( 2\left(\frac{\partial \overline{U}}{\partial \overline{X}}\right)^2 + 2\left(\frac{\partial \overline{V}}{\partial \overline{Y}}\right)^2 + \left(\frac{\partial \overline{U}}{\partial \overline{Y}} + \frac{\partial \overline{V}}{\partial \overline{X}}\right)^2 \right) \\
+ \frac{\sigma_{nf}B_0^2}{(\rho c_p)_{nf}} (\overline{U} + c)^2 + \frac{k_{nf}}{(\rho c_p)_{nf}} \left(\frac{\partial^2 \overline{T}}{\partial \overline{X}^2} + \frac{\partial^2 \overline{T}}{\partial \overline{Y}^2}\right)
\end{cases}, (10)$$

Now, the non-dimensionalized variables are being introduced.

$$\begin{pmatrix} X \\ Y \end{pmatrix} = \begin{pmatrix} \frac{\overline{X}}{\lambda} \\ \frac{\overline{Y}}{W_{1}} \end{pmatrix}, \begin{pmatrix} U \\ V \end{pmatrix} = \begin{pmatrix} \frac{\overline{U}}{c} \\ \frac{\overline{V}}{V} \end{pmatrix}, \tau = \frac{w_{1}}{\lambda}, \\
\frac{\overline{V}}{V} = \begin{pmatrix} \frac{w_{1}^{2} \overline{P}}{\lambda c \mu_{0}} \\ \Theta \Delta T + T_{o} \end{pmatrix}, \Delta T = T_{1} - T_{0}$$
(11)

When Eq. (11) is substituted into equations 7–10, we obtained:

$$\frac{\partial U}{\partial X} + \frac{\partial V}{\partial Y} = 0,\tag{12}$$

$$\Lambda_{1} \operatorname{Re} \tau \left( U \frac{\partial U}{\partial X} + V \frac{\partial U}{\partial Y} \right) = \begin{cases}
-\frac{\partial P}{\partial X} + \Lambda_{2} \left( \frac{\partial^{2} U}{\partial Y^{2}} + \tau^{2} \frac{\partial^{2} U}{\partial X^{2}} \right) \\
+ Gr \Lambda_{3} \Theta - \Lambda_{4} M_{h}^{2} (U + 1),
\end{cases}$$
(13)

$$\Lambda_{1} \operatorname{Re} \tau^{3} \left( U \frac{\partial V}{\partial X} + V \frac{\partial V}{\partial Y} \right) = -\frac{\partial P}{\partial Y} + \tau^{2} \Lambda_{2} \left( \frac{\partial^{2} V}{\partial Y^{2}} + \tau^{2} \frac{\partial^{2} V}{\partial X^{2}} \right), \tag{14}$$

$$\operatorname{RePr} \tau \Lambda_{5} \left( U \frac{\partial \Theta}{\partial X} + V \frac{\partial \Theta}{\partial Y} \right) = \begin{cases} \Lambda_{6} \left( \frac{\partial^{2} \Theta}{\partial Y^{2}} + \tau^{2} \frac{\partial^{2} \Theta}{\partial X^{2}} \right) \\ + \operatorname{Pr} \operatorname{Ec} \Lambda_{2} \left( \left( \left( \frac{\partial V}{\partial Y} \right)^{2} + \left( \frac{\partial U}{\partial X} \right)^{2} \right) 2 \tau^{2} + \left( \frac{\partial U}{\partial Y} + \frac{\partial V}{\partial X} \tau^{2} \right)^{2} \right) \\ + \Lambda_{4} M_{b}^{2} \operatorname{Ec} \operatorname{Pr} \left( U + 1 \right)^{2}. \end{cases}$$

$$(15)$$

Here (X, Y) and (U, V) correspondingly denotes dimensionless space coordinates and velocity components, whereas  $\Theta$  shows the dimensionless temperature of the nanofluid. Whereas the symbols  $(\Lambda_1, \Lambda_2, \Lambda_3, \Lambda_4, \Lambda_5, \Lambda_6)$  are defines as given below

$$\Lambda_{1} = \frac{\rho_{nf}}{\rho_{bf}}, \Lambda_{2} = \frac{\mu_{nf}}{\mu_{bf}}, \Lambda_{3} = \frac{(\rho\beta)_{nf}}{(\rho\beta)_{bf}}, 
\Lambda_{4} = \frac{\sigma_{nf}}{\sigma_{bf}}, \Lambda_{5} = \frac{(\rho c_{p})_{nf}}{(\rho c_{p})_{bf}}, \Lambda_{6} = \frac{k_{nf}}{k_{bf}}.$$
(16)

By introducing a stream function  $\overline{\psi} = \psi/cw_1$  with  $U = \frac{\partial \psi}{\partial Y}$ ,  $V = -\frac{\partial \psi}{\partial X}$  and using a long wave length approximation  $(\tau \ll 1)$ , Eqs. 13–15 take the following form

$$\Lambda_2 \frac{\partial^2}{\partial Y^2} \left( \frac{\partial \psi}{\partial Y} \right) + Gr \Lambda_3 \Theta - \Lambda_4 M_h^2 \left( \frac{\partial \psi}{\partial Y} + 1 \right) = \frac{\partial P}{\partial X} \tag{17}$$

$$\frac{\partial P}{\partial Y} = 0,\tag{18}$$

$$\frac{\partial^2 \Theta}{\partial Y^2} \Lambda_6 + \Pr \Lambda_2 Ec \left( \frac{\partial^2 \psi}{\partial Y^2} \right)^2 + \Lambda_4 M_h^2 Ec \Pr \left( \frac{\partial \psi}{\partial Y} + 1 \right)^2 = 0.$$
 (19)

As given below, the momentum and heat equations are transformed when the pressure gradient is eliminated.

$$\Lambda_2 \frac{\partial^3}{\partial Y^3} \left( \frac{\partial \psi}{\partial Y} \right) + Gr \Lambda_3 \frac{\partial \Theta}{\partial Y} - \Lambda_4 M_h^2 \left( \frac{\partial^2 \psi}{\partial Y^2} \right) = 0 \tag{20}$$

$$\Lambda_{6} \frac{\partial^{2} \Theta}{\partial Y^{2}} + \operatorname{Pr} E c \Lambda_{2} \left( \frac{\partial^{2} \psi}{\partial Y^{2}} \right)^{2} + \Lambda_{4} M_{h}^{2} E c \operatorname{Pr} \left( \frac{\partial \psi}{\partial Y} + 1 \right)^{2} = 0.$$

$$(21)$$

Here

$$Gr = \frac{(\rho \beta)_{bf} g \Delta T w_1^2}{c \mu_{bf}} (Grash of \ number), Ec = \frac{c^2}{\left(c_p\right)_{bf} \Delta T} (Eckert \ number),$$

$$M_h^2 = \frac{B_0^2 w_1^2 \sigma_{bf}}{\mu_{bf}} (\textit{magnetic parameter}) \text{ and } \Pr = \left(\frac{\mu c_p}{k}\right)_{bf} (\textit{Prandtl number}).$$

The unit less boundary conditions are

$$\begin{cases} \psi = +\frac{F}{2}, \frac{\partial \psi}{\partial y} = -1, \Theta = 0 & \text{at} \quad \omega_1(X) = 1 + a\cos(2\pi X), \\ \psi = -\frac{F}{2}, \frac{\partial \psi}{\partial y} = -1, \Theta = 1 & \text{at} \quad \omega_2(X) = -d - b\cos(2\pi X + \varphi). \end{cases}$$
(22)

**Table 1**Presents the correlations regarding the thermophysical properties of nanofluid [52,53].

| Properties                    | without aggregation  | with aggregation   |  |
|-------------------------------|--|--|--|
| Thermal conductivity          | $k_{nf} = k_{bf} iggl\{ rac{(k_p + 2k_{bf}) + 2(k_p - k_{bf})\Phi}{(k_p + 2k_{bf}) - (k_p - k_{bf})\Phi} iggr\},$                           | $k_{nf} = k_{bf} iggl\{ rac{(k_a + 2k_{bf}) + 2(k_a - k_{bf})\Phi_a}{(k_a + 2k_{bf}) - (k_a - k_{bf})\Phi_a} iggr\},$   |  |
| Heat<br>capacitance           | $\left( ho c_{p} ight)_{nf} = \left\{egin{array}{l} (1-\Phi) \left( ho c_{p} ight)_{bf} \ +\Phi \left( ho c_{p} ight)_{p} \end{array} ight.$ | $\left( ho c_{p} ight)_{nf} = \left\{egin{array}{l} \left(1-\Phi_{a} ight)\left( ho c_{p} ight)_{bf} \ +\Phi_{a}\left( ho c_{p} ight)_{bf}\left( ho c_{p} ight)_{p} \end{array} ight.$ |  |
| Electric<br>conductivity      | $rac{\sigma_{nf}}{\sigma_{bf}} = 1 + rac{3\Phi(\sigma-1)}{2+\sigma-\Phi(\sigma-1)}$  | $rac{\sigma_{nf}}{\sigma_{bf}} = 1 + rac{3(\sigma-1)\Phi_a}{2+\sigma-(\sigma-1)\Phi_a}$  |  |
|                               | where $\sigma = rac{\sigma_p}{\sigma_{bf}}$   | where $\sigma = rac{\sigma_p}{\sigma_{bf}}$   |  |
| Density                       | $rac{ ho_{nf}}{ ho_{bf}}=(1-\Phi)+\Phirac{ ho_{p}}{ ho_{bf}}$  | $rac{ ho_{nf}}{ ho_{bf}} = (1-\Phi_a) + \Phi_a rac{ ho_p}{ ho_{bf}}$   |  |
| Dynamic viscosity             | $rac{\mu_{nf}}{\mu_{bf}}=rac{1}{(1-\mathbf{\Phi})^{2.5}}$  | $rac{\mu_{nf}}{\mu_{bf}} = \left(1 - rac{\Phi\left(rac{r_a}{r_p} ight)^{3-D}}{\Phi_m} ight)^{-[e]} rac{\Phi_m}{}$  |  |
| Thermal expansion coefficient | $( hoeta)_{n\!f} = iggl[ \Phi rac{( hoeta)_p}{( hoeta)_{b\!f}} + (1-\Phi) iggr] ( hoeta)_{b\!f}$  | $( hoeta)_{nf} = \left[\Phi_a rac{( hoeta)_p}{( hoeta)_{bf}} + (1 - \Phi_a) ight] ( hoeta)_{bf}$  |  |

In boundary conditions (22) here unit less time-mean flow rate F (observed in wavy frame) and  $\chi$  (observed in stationary frame) exhibit a relationship defined by the following equation

$$F = \chi - d - 1. \tag{23}$$

### 2.1. Modeling the features of nanofluids with nanoparticles aggregation

The precise modeling of the characteristics of  $TiO_2/H_2O$  nanofluid (NF) can be achieved through the kinematics of nanoparticle aggregation. In their study, Chen et al. [52] provided a comprehensive description of the models that were employed for the  $TiO_2/EG$  NF system, considering the impact of nanoparticle aggregation. The theoretical models and correlations exhibited a high level of concurrence with the experimental findings. Table 1 presents a complete review and comparison of standard NF models that do not consider the impact for the influence of NP aggregation alongside the models introduced by Chen et al. [52].

# 2.1.1. Solid volume fraction with aggregation effect

The existence of non-uniformity in the distribution of NPs within aggregate (agg.) structures implies that the density of NPs changes in accordance with a power law i.e. density of NPs changes with the radial position. The determination of the solid volume fraction of NP agg. Denoted as  $\Phi_a$ , is calculated through the relationship outlined below [52,53]

$$\Phi_a = \Phi\left(\frac{r_a}{r_p}\right)^{3-D} \tag{24}$$

Within the given framework, the symbol D represents the constant fractal index, while the symbol  $\Phi$  denotes the solid volume fraction of isolated nanoparticles (NPs). Additionally,  $r_a$  signifies the radius of NP agg., and  $r_p$  corresponds to the radius of isolated NPs. Chen et al. [39] have provided noteworthy findings regarding the appropriate values for D (the fractal index) and  $r_a$  (radius of nanoparticle (NP) agg.). Specifically, they have documented that D has a value of 1.8, while  $r_a$  is equal to 3.34 times the radius of individual nanoparticles  $(r_p)$ ..

### 2.1.2. Effective viscosity with NPs aggregation

The accurate determination of the viscosity of  $TiO2/H_2O$  nanofluids is achieved through the modification of the Krieger-Dougherty model, which considers the presence of nanoparticle aggregates. The updated model effectively calculates the effective viscosity of  $TiO_2/H_2O$  with aggregates of nanoparticles. Presented below is the new conceptual framework for the characterization of viscosity [52,53].

$$\frac{\mu_{nf}}{\mu_{bf}} = \left(1 - \frac{\Phi_a}{\Phi_m}\right)^{-[\varepsilon] \Phi_m} \tag{25}$$

Within the present framework, the variable  $[\varepsilon]$  denotes the intrinsic viscosity, assuming a precise numerical value of  $[\varepsilon]=2.5$ , whereas  $\Phi_m$  is assigned a value of 0.605.

# 2.1.3. Effective thermal conductivity with nanoparticles aggregation

The conventional Maxwell equation is typically used to evaluate the thermal conductivity of different nanofluids (NFs) or homogeneous mixtures

$$k_{nf} = k_{bf} \left\{ \frac{(k_p + 2k_{bf}) + 2\Phi(k_p - k_{bf})}{(k_p + 2k_{bf}) - \Phi(k_p - k_{bf})} \right\}. \tag{26}$$

The symbols  $k_{bf}$ ,  $k_{nf}$  and  $k_p$  and for the thermal conductivities of the working fluid, nanofluid (NF), and nanoparticles (NPs), respectively. Nevertheless, the previously indicated traditional Maxwell model fails to take into account the impact of NPs agg. on thermal conductivity. The Bruggeman model should be incorporated into the Maxwell model, as suggested by Chen et al. [52]. This will provide an updated model that takes NPs aggregation into account. The thermal conductivity of NPs agg. is estimated using the model documented by Bruggeman. According to Chen et al. [52] the following is the representation of the modified Maxwell model that takes thermal conductivity with NPs aggregates

$$k_{nf} = k_{bf} \left\{ \frac{(k_a + 2k_{bf}) + 2\Phi_a(k_a - k_{bf})}{(k_a + 2k_{bf}) - \Phi_a(k_a - k_{bf})} \right\}.$$
(27)

The thermal conductivity of nanofluid, aggregates of  $TiO_2$  nanoparticles (NPs), and water are denoted by  $k_{nf}$ ,  $k_a$  and  $k_{bf}$ . Furthermore, Chen et al. [52] reported that the Bruggeman model determines the thermal conductivity of NPs aggregates in the following way

$$k_a = 0.25 \left[ (3\Phi_i - 1) \frac{k_p}{k_f} + (3(1 - \Phi_i) - 1) + \left\{ \left( (3\Phi_i - 1) \frac{k_p}{k_f} + (3(1 - \Phi_i) - 1) \right)^2 + 8 \frac{k_p}{k_f} \right\}^{0.5} \right], \tag{28}$$

Here,  $\Phi_i = \left(\frac{r_a}{r_p}\right)^{D-3}$ . Further, the quantitative data regarding the thermophysical characteristics of water (H<sub>2</sub>O) and TiO<sub>2</sub> nanoparticles

can be seen from Table 2.

### 3. Minimization of entropy generation

The phenomenon of entropy formation in a flow of dissipative nanofluid within a wavy channel, considering the influence of magnetic dissipation is expressed as [42–46].

$$\widehat{\hat{\mathsf{S}}}^{"}_{Gen} = \begin{cases}
\frac{k_{nf}}{T^{*2}} \left( \left( \frac{\partial T^{*}}{\partial X^{*}} \right)^{2} + \left( \frac{\partial T^{*}}{\partial Y^{*}} \right)^{2} \right) + U^{*2} \frac{\sigma_{nf}}{T^{*}} B_{o}^{2} \\
+ \frac{2\mu_{nf}}{T^{*}} \left( \left( \frac{\partial U^{*}}{\partial X^{*}} \right)^{2} + \left( \frac{\partial V^{*}}{\partial Y^{*}} \right)^{2} + \frac{1}{2} \left( \frac{\partial V^{*}}{\partial X^{*}} + \frac{\partial U^{*}}{\partial Y^{*}} \right)^{2} \right),
\end{cases} (29)$$

Utilizing the Galilean transformations defined in (6), the expression (29) becomes

$$\dot{S}_{GEN}^{"} = \begin{cases}
\frac{k_{nf}}{\overline{T}^2} \left( \left( \frac{\partial \overline{T}}{\partial \overline{X}} \right)^2 + \left( \frac{\partial \overline{T}}{\partial \overline{Y}} \right)^2 \right) + \frac{\sigma_{nf}}{\overline{T}} B_o^2 (\overline{U} + c)^2 \\
+ \frac{\mu_{nf}}{\overline{T}} \left( 2 \left( \frac{\partial \overline{U}}{\partial \overline{X}} \right)^2 + 2 \left( \frac{\partial \overline{U}}{\partial \overline{Y}} \right)^2 + \left( \frac{\partial \overline{U}}{\partial \overline{Y}} + \frac{\partial \overline{V}}{\partial \overline{X}} \right)^2 \right).
\end{cases} (30)$$

By using Eq. (11), the entropy generation number (Ns) in an inertial moving frame takes the following form

$$Ns = \frac{\dot{S}_{GEN}^{"}}{\left(\dot{S}_{GEN}^{"}\right)_{0}} = \begin{cases} \frac{\Lambda_{6}}{\left(\Theta + \theta_{d}\right)^{2}} \left(\left(\frac{\partial\Theta}{\partial Y}\right)^{2} + \tau^{2}\left(\frac{\partial\Theta}{\partial X}\right)^{2}\right) \\ + \Lambda_{4}\frac{M_{h}^{2} \operatorname{Pr} Ec}{\left(\Theta + \theta_{d}\right)} \left(U + 1\right)^{2} \\ + \frac{2 \operatorname{Pr} Ec}{\left(\Theta + \theta_{d}\right)} \left(\tau^{2}\left(\left(\frac{\partial V}{\partial Y}\right)^{2} + \left(\frac{\partial U}{\partial X}\right)^{2}\right) + \frac{1}{2}\left(\frac{\partial U}{\partial Y} + \frac{\partial V}{\partial X}\tau\right)^{2}\right). \end{cases}$$
(31)

Introducing  $\psi(X,Y)$  in such a way that  $U=\frac{\partial \psi}{\partial Y}$ ,  $V=-\frac{\partial \psi}{\partial X}$  and utilizing long wave length approximation  $(\tau\ll 1)$ , (31) takes the following form

$$Ns = \begin{cases} \frac{\Lambda_6}{(\Theta + \theta_d)^2} \left(\frac{\partial \Theta}{\partial Y}\right)^2 + \Lambda_4 \frac{M_h^2 \operatorname{Pr} Ec}{(\Theta + \theta_d)} \left(\frac{\partial \psi}{\partial Y} + 1\right)^2 \\ + \frac{\operatorname{Pr} Ec}{(\Theta + \theta_d)} \left(\frac{\partial^2 \psi}{\partial Y^2}\right)^2 \end{cases}$$
(32)

The notation  $(\hat{S}_{GEN}^{'''})_0$  and  $\theta_d$  used in (32) respectively stand for characteristic entropy generation and temperature difference parameter and defines as follows:

$$\left(\hat{S}_{GEN}^{"'}\right)_0 = \frac{k_{bf}}{w^2}, \theta_d = \frac{T_0}{\Delta T}.$$
(33)

# 4. Numerical Strategy: differential quadrature method (DQM)

Using the differential quadrature method [54–56], the subsequent system of dimensionless nonlinear differential equations is numerically solved.

**Table 2**Numerical values of thermophysical properties.

|                          | $\sigma(\Omega.m)^{-1}$ | $\rho \big( \mathit{kgm}^{-3} \big)$ | k(W/KgK) | $c_p(W/mK)$ | $\beta(1/K)$        |
|--------------------------|-------------------------|--------------------------------------|----------|-------------|---------------------|
| Water (H <sub>2</sub> O) | 0.05                    | 997.1                                | 0.613    | 4179        | $21\times 10^{-5}$  |
| $TiO_2$                  | $2.38\times 10^6$       | 4250                                 | 8.9538   | 686.2       | $1.05\times10^{-5}$ |

$$S_{NL}(X,Y) = \begin{cases} \psi = -\frac{F}{2}, \frac{\partial \psi}{\partial Y} = -1, Y = \omega_2(X), \\ \Lambda_2 \frac{\partial^3}{\partial Y^3} \left( \frac{\partial \psi}{\partial Y} \right) + Gr \Lambda_3 \frac{\partial \Theta}{\partial Y} - \Lambda_4 M_h^2 \left( \frac{\partial^2 \psi}{\partial Y^2} \right) = 0 \\ \psi = \frac{F}{2}, \frac{\partial \psi}{\partial Y} = -1 \text{ at } Y = \omega_1(X), \\ \Theta = 1 \text{ at } Y = \omega_2(X), \\ \Lambda_6 \frac{\partial^2 \Theta}{\partial Y^2} + \Pr Ec \Lambda_2 \left( \frac{\partial^2 \psi}{\partial Y^2} \right)^2 + \Lambda_4 M_h^2 Ec \Pr \left( \frac{\partial \psi}{\partial Y} + 1 \right)^2 = 0 \\ \Theta = 0, \text{ at } Y = \omega_1(X), \end{cases}$$

$$(34)$$

To facilitate DQM implementation, the following additional transformations are used [54].

$$\begin{cases} Y = \xi(\omega_1(X) - \omega_2(X)) + \omega_2(X), \\ \psi(X, Y) = \widetilde{\psi}(X, \xi) + \psi(X, \omega_2(X) + \xi(\omega_1(X) - \omega_2(X))), \\ \Theta(X, Y) = \widetilde{T}(X, \xi) = T(X, \omega_2(X) + \xi(\omega_1(X) - \omega_2(X))), \end{cases}$$
(35)

Keeping the transformations (35) in mind, the nth-order derivative of  $\psi(X,Y)$  and T(X,Y) can be represented as [54]

$$\begin{cases}
\frac{\partial^n \psi(X,Y)}{\partial Y^n} = \frac{1}{(\omega_1(X) - \omega_2(X))^n} \frac{\partial^n \widetilde{\psi}(X,\xi)}{\partial \xi^n}, \\
\frac{\partial^n \Theta(X,Y)}{\partial Y^n} = \frac{1}{(\omega_1(X) - \omega_2(X))^n} \frac{\partial^n \widetilde{T}(X,\xi)}{\partial \xi^n}.
\end{cases}$$
(36)

Based on (35) and (36), we can express the nonlinear system  $(S_{NL}(X,\xi))$  as follows

$$S_{NL}(X,\xi) = \begin{cases} \widetilde{\psi}(X,\xi=0) = -\frac{F}{2}, \left(\frac{\partial \widetilde{\psi}}{\partial \xi}\right)_{\xi=0} = -\Delta, where \ \Delta = \omega_{1}(X) - \omega_{2}(X), \\ L_{\widetilde{\psi}}(\widetilde{\psi},\widetilde{T}) + N_{\widetilde{\psi}}(\widetilde{\psi},\widetilde{T}) = 0, \\ \widetilde{\psi}(X,\xi=1) = \frac{F}{2}, \left(\frac{\partial \widetilde{\psi}}{\partial \xi}\right)_{\xi=1} = -\Delta, where \ \Delta = \omega_{1}(X) - \omega_{2}(X), \\ \widetilde{T}(X,\xi=0) = 1, \\ L_{\widetilde{T}}(\widetilde{\psi},\widetilde{T}) + N_{\widetilde{T}}(\widetilde{\psi},\widetilde{T}) + \Lambda_{4}M_{h}^{2}Ec \ Pr = 0, \\ \widetilde{T}(X,\xi=1) = 0, \end{cases}$$

$$(37)$$

In the above system  $(S_{NL}(X,\xi))$ , the linear  $L_{\widetilde{\psi}}(\widetilde{\psi},\widetilde{T}), L_{\widetilde{T}}(\widetilde{\psi},\widetilde{T})$  and nonlinear  $N_{\widetilde{\psi}}(\widetilde{\psi},\widetilde{T}), N_{\widetilde{T}}(\widetilde{\psi},\widetilde{T})$  parts are defined as follows:

$$L_{\tilde{\psi}}(\widetilde{\psi},\widetilde{T}) = \frac{\Lambda}{\Delta^4} \left( \frac{\partial^4 \widetilde{\psi}}{\partial^4 \xi} \right) + \frac{Gr\Lambda_3}{\Delta} \frac{\partial \widetilde{T}}{\partial \xi} - \frac{\Lambda_4 M_h^2}{\Delta^2} \left( \frac{\partial^2 \widetilde{\psi}}{\partial \xi^2} \right), \tag{38}$$

$$L_{\tilde{T}}(\eta,\chi) = \frac{\Lambda_6}{\Delta^2} \frac{\partial^2 \widetilde{T}}{\partial \xi^2} + \Lambda_4 M^2 Ec \, \Pr\left(\frac{2}{\Delta} \frac{\partial \widetilde{\psi}}{\partial \xi}\right), \tag{39}$$

$$N_{\widetilde{w}}(X,\widetilde{\psi}) = 0 \tag{40}$$

$$N_{\tilde{T}}(X,\xi) = \frac{\Pr{Ec\Lambda_2}}{\Delta^4} \left(\frac{\partial^2 \widetilde{\psi}}{\partial \xi^2}\right)^2 + \frac{\Lambda_4 M_h^2 \Pr{Ec}}{\Delta^2} \left(\frac{\partial \widetilde{\psi}}{\partial \xi}\right)^2. \tag{41}$$

With the help of Eqs. (35) and (36), Eq. (32) take the following form:

$$Ns(X,\xi) = \begin{cases} \frac{\Lambda_6}{\Delta^2 (\widetilde{T} + \theta_d)^2} \left(\frac{\partial \widetilde{T}}{\partial \xi}\right)^2 + \Lambda_4 \frac{M_h^2 \operatorname{Pr} Ec}{(\widetilde{T} + \theta_d)} \left(\frac{1}{\Delta} \frac{\partial \widetilde{\psi}}{\partial \xi} + 1\right)^2 + \\ \frac{Br}{\Delta^4 (\widetilde{T} + \theta_d)} \left(\frac{\partial^2 \widetilde{\psi}}{\partial \xi^2}\right)^2 \end{cases}$$
(42)

Moreover, as mentioned earlier, the longitudinal pressure gradient can be formulated in the following manner

M.I. Afridi et al.

$$\frac{\partial \widetilde{P}}{\partial X} = \Lambda_2 \left( \frac{1}{\Delta^3} \frac{\partial^3 \widetilde{\psi}}{\partial \xi^3} \right) + Gr \Lambda_3 \widetilde{T} - \Lambda_4 M_h^2 \left( \frac{1}{\Delta} \frac{\partial \widetilde{\psi}}{\partial \xi} + 1 \right)$$
(43)

Here

$$P(X,Y) = \widetilde{P}(X,\xi) = P(X,\xi(\omega_1(X) - \omega_2(X) + \omega_2(X))). \tag{44}$$

Below is the non-uniform discretization of the computational domain [0,1].

$$\xi_i = \frac{1}{2} \left( 1 + \cos\left(\frac{(1-i)\pi}{N-1}\right) \right). \tag{45}$$

Here, N displays the overall number of Gauss-Lobatto mesh points and  $1 \le i \le N$ . In discrete form, the derivatives of  $\widetilde{\psi}(X,\xi)$  and  $\widetilde{T}(X,\xi)$  at grid points  $\xi_i$  are defined as given below

$$\begin{cases}
\frac{\partial^{p} \widetilde{\psi}}{\partial \xi^{p}} \Big)_{\xi=\xi_{i}} = \sum_{j=1}^{N} D_{ij}^{(p)} \widetilde{\psi}(X, \xi = \xi_{i}) = \sum_{j=1}^{N} D_{ij}^{(p)} \widetilde{\psi}_{j}(X), 1 \leq i, j \leq N, \\
\frac{\partial^{p} \widetilde{T}}{\partial \xi^{p}} \Big)_{\xi=\xi_{i}} = \sum_{j=1}^{N} D_{ij}^{(p)} \widetilde{T}(X, \xi = \xi_{i}) = \sum_{j=1}^{N} D_{ij}^{(p)} \widetilde{T}_{j}(X), 1 \leq i, j \leq N.
\end{cases}$$
(46)

here,  $D_{ij}^{(p)}$  shows quadrature weighting coefficients. Following Nayak et al. [41], the weighted coefficients can be written as given below

$$\begin{cases}
D_{ij}^{(p)} = \frac{\prod_{k=1, k \neq i}^{N} (\xi_i - \xi_k)}{(\xi_i - \xi_j) \prod_{k=1, k \neq j}^{N} (\xi_j - \xi_k)}, & \text{for } m = 1, i \neq j \text{ and } 1 \leq i, j \leq N, \\
D_{ij}^{(p)} = n \left( D_{ii}^{(p-1)} D_{ij}^{(1)} - \frac{D_{ij}^{(p-1)}}{(\xi_i - \xi_j)} \right), & \text{for } m \geq 2, i \neq j \text{ and } 1 \leq i, j \leq N, \\
M_{ij}^{(p)} = -\sum_{k=1, j \neq i}^{N} M_{ij}^{(p)} & \text{for } i = j,
\end{cases}$$
(47)

By substituting the discretized representation of both the variables and its corresponding derivatives within system (37), the resultant discretized system is obtained as follows

$$S_{NL}(X,\xi_{i}) = \begin{cases} \widetilde{\psi}_{i}(X) + F / 2 = 0, \sum_{j=1}^{N} D_{ij}^{(1)} \widetilde{\psi}_{j}(\eta) + \Delta = 0, \text{ when } i = 1, \\ L_{\widetilde{\psi}_{i}}(\widetilde{\psi}_{i}(X), \widetilde{T}_{i}(X)) + N_{\widetilde{\psi}_{i}}(\widetilde{\psi}_{i}(X), \widetilde{T}_{i}(X)) = 0, \text{ for } 3 \leq i \leq N - 2, \\ \widetilde{\psi}_{i}(\eta) - \frac{F}{2} = 0, \sum_{j=1}^{N} D_{ij}^{(1)} \widetilde{\psi}_{j}(X) + \Delta = 0, \text{ when } i = N, \\ \widetilde{T}_{i}(X) = 1, \text{ when } i = 1, \\ L_{\widetilde{T}_{i}}(\widetilde{\psi}_{i}(X), \widetilde{T}_{i}(X)) + N_{\widetilde{T}_{i}}(\widetilde{\psi}_{i}(X), \widetilde{T}_{i}(X)) + \Lambda_{4} M_{h}^{2} Ec \Pr = 0, \text{ for } 2 \leq i \leq N - 1 \\ \widetilde{T}_{j}(X) = 0, \text{ when } i = N. \end{cases}$$

$$(48)$$

in which

$$\mathsf{L}_{\widetilde{\psi}_i}(\widetilde{\psi}_i(X),\widetilde{T}_i(X)) = \frac{\Lambda}{\Delta^4} \sum_{i=1}^N D_{ij}^{(4)} \widetilde{\psi}_j(X) + \frac{Gr\Lambda_3}{\Delta} \sum_{i=1}^N D_{ij}^{(1)} \widetilde{T}_j(X) - \frac{\Lambda_4 M_h^2}{\Delta^2} \left( \sum_{i=1}^N D_{ij}^{(2)} \widetilde{\psi}_j(X) \right), \tag{49}$$

$$\mathsf{L}_{\tilde{T}_{l}}(\widetilde{\psi}_{i}(X),\widetilde{T}_{i}(X)) = \frac{\Lambda_{6}}{\Delta^{2}} \sum_{i=1}^{N} D_{ij}^{(2)} \widetilde{T}_{j}(X) + \Lambda_{4} M^{2} Ec \ \mathsf{Pr}\left(\frac{2}{\Delta} \sum_{i=1}^{N} D_{ij}^{(1)} \widetilde{\psi}_{j}(X)\right), \tag{50}$$

$$N_{\widetilde{\psi}_i}(\widetilde{\psi}_i(X), \widetilde{T}_i(X)) = 0 \tag{51}$$

$$N_{\widetilde{T}_{i}}(\widetilde{\psi}_{i}(X),\widetilde{T}_{i}(X)) = \frac{\operatorname{Pr} Ec\Lambda_{2}}{\Delta^{4}} \left( \sum_{j=1}^{N} D_{ij}^{(2)} \widetilde{\psi}_{j}(X) \right)^{2} + \frac{\Lambda_{4} M_{h}^{2} \operatorname{Pr} Ec}{\Delta^{2}} \left( \sum_{j=1}^{N} D_{ij}^{(1)} \widetilde{\psi}_{j}(X) \right)^{2}.$$

$$(52)$$

We have discretized nonlinear system  $S_{NL}(X, \xi_i)$  and resulting into a system of 2N nonlinear algebraic equations. Therefore, we utilized the Newton-Raphson Method to solve the discretized system iteratively. Furthermore, the numerical calculation of the pressure gradient and entropy generation can be conducted as outlined below:

$$\frac{\partial \widetilde{P}}{\partial X} = \Lambda_2 \left( \frac{1}{\Delta^3} \sum_{j=1}^N D_{ij}^{(3)} \widetilde{\psi}_j(X) \right) + Gr \Lambda_3 \widetilde{T}_i(X) - \Lambda_4 M_h^2 \left( \frac{1}{\Delta} \sum_{j=1}^N D_{ij}^{(1)} \widetilde{\psi}_j(X) + 1 \right)$$
 (53)

$$Ns(X, \xi_{i}) = \begin{cases} \frac{\Lambda_{6}}{\Delta^{2} (\widetilde{T}_{i}(X) + \theta_{d})^{2}} \left( \sum_{j=1}^{N} D_{ij}^{(1)} \widetilde{T}_{j}(X) \right)^{2} + \\ \Lambda_{4} \frac{M_{h}^{2} \operatorname{Pr} Ec}{(\widetilde{T}_{i}(X) + \theta_{d})} \left( \frac{1}{\Delta} \sum_{j=1}^{N} D_{ij}^{(1)} \widetilde{\psi}_{j}(X) + 1 \right)^{2} + \\ \frac{Br}{\Delta^{4} (\widetilde{T}_{i}(X) + \theta_{d})} \left( \sum_{j=1}^{N} D_{ij}^{(2)} \widetilde{\psi}_{j}(X) \right)^{2}, \end{cases}$$
(54)

The simulation in MATLAB is conducted through the application of the generalized differential quadrature method. The flow chart as depicted in Fig. 2 outlines the essential steps of the GDQM.

### 5. Results and discussion

The aim of this section is to investigate the impact of pertinent factors including the Eckert number EC {0.0,0.05,0.1}, solid volume fraction  $\Phi$ {0.01,0.02,0.03}, Grashof number GC{1,2,3}, magnetic parameter  $M_h$  {0.2,1.2,2.2} and temperature difference parameter  $\theta_d$  {0.5,1.5,2.5} on velocity U(X,Y), temperature  $\Theta(X,Y)$ , entropy generation Ns(X,Y) heat transfer rate and pressure gradient  $\frac{dP}{dX}$ . It is

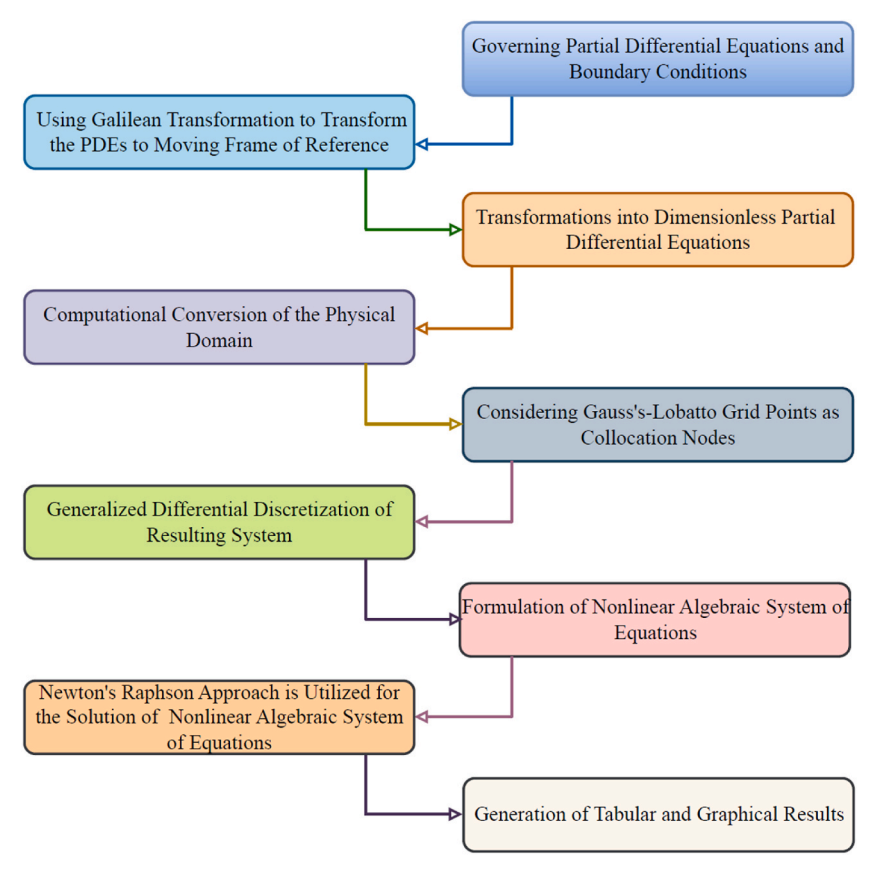


Fig. 2. Flow chart, utilization of GDQM.

noted that as each flow parameter is altered, the remaining parameters are held constant as  $M_h=1.5$ , Gr=2.0, X=0.1, Ec=0.05,  $\Phi=0.04$  and  $\theta_d=1.5$ . Prandtl number Pr for the base fluid, water, has a fixed value of 6.83 throughout the analysis, Moreover, values of the parameters related to channel geometry namely, amplitudes of the waves, channel width and phase difference are also kept fixed at a=0.5, b=0.5, d=0.9 and  $\varphi=\pi/4$ . A comparative analysis of key quantities—including velocity, pressure gradient, temperature, trapping phenomena, heat transfer, and volumetric entropy generation rates—has been conducted for the peristaltic flow of nanofluids, both with and without nanoparticle aggregation.

# 5.1. Effects of nanoparticles aggregation (NPs agg.)

Fig (3)-(23) show that nanoparticle aggregation significantly affects heat transfer rate, pressure gradient, velocity, temperature, and entropy generation within the fluid. Specifically, Fig (3)-(5) reveal that velocity profiles in the central region of the channel decrease with nanoparticle aggregation. Physically, nanofluids exhibit elevated viscosity on account of the scattered nanoparticles, whose presence augments resistance to flow and accordingly slows the fluid motion. Fig (6) (8) point out that the thermal profile is higher with nanoparticle aggregation because of high effective thermal conductivity. Additionally, Fig (9)-(12) demonstrate that entropy generation is higher in nanofluids with aggregated nanoparticles compared to those without aggregation (see Fig. 7).

# 5.2. Axial pressure gradient

Fig. 3 depicts the effect of the solid volume fraction  $(\Phi)$  on the axial pressure gradient, showing that the magnitude of  $\frac{dP}{dX}$  in absolute sense is highest for nano fluid without aggregation. Additionally, this magnitude enhances as solid volume fraction increases. Fig. 4 depicts the change in the axial pressure gradient  $\left(\frac{dP}{dX}\right)$  with change in Hartman number  $(M_h)$  and it is noticed that the absolute strength of  $\frac{dP}{dX}$  intensifies as the Hartman number increases. Further, the magnitude of  $\frac{dP}{dX}$  in absolute sense is lowest with nanoparticles aggregation. Figs. 5 and 6 respectively depict the influence of Grashof (Gr) and Eckert number on  $\frac{dP}{dX}$ , indicating that the magnitude of  $\frac{dP}{dX}$  decline with rising magnitudes of Grashof and Eckert number. It is significant to note that the pressure gradient is higher for the nanofluid when considering the effect of nanoparticle aggregation compared to the nanofluid without accounting for this effect.

### 5.3. Trapping phenomena

Fig. 7 (a) and (b) respectively show how the streamlines vary with increasing magnetic parameter by considering the nanoparticles aggregation and without accounting for this effect. When the strength of the magnetic field is increased, the size of the trapped bolus reduces. This occurs, because the larger field is more effective in contracting the bolus, an effect driven by the relative dynamics of the flow. In addition, under the influence of the magnetic force, more fluid tends to flow into the right side of channel's center, as before.

# 5.4. Velocity profiles

The influence of the parameters  $(\Phi, M_h, Gr, Ec)$  on velocity profiles is demonstrated in Figs. (8)-(11) respectively. An elevated solid volume fraction, as illustrated in Fig. 8, leads to a decrement in the velocity distribution at the central region of the channel. The velocity is declining at the center and upsurge near the deformable walls with enhancing the magnetic number  $(M_h)$  as shown in Fig. 9. The intensified magnetic field applies a resistance force on the fluid, effectively diminishing the fluid velocity. The Lorentz forces act in opposition to the flow, resulting in increased resistance and decreased velocity in the central region of the channel. At the center, the nanofluid with aggregation has greater velocity as compared to the nanofluid without the agg. From Fig. 10, the velocity of nanofluid upsurge at the center and near the left wall with growing values of Grashof number (Gr). The decline in velocity profile is observed towards the right wall. At the center and towards the left wall, lower velocity is observed corresponding to the nanofluid without the nanoparticle's aggregation. Fig. 11 establishes that as the Eckert number (Ec) rises, the velocity declines towards the walls and rises at the center. The thermal conductivity enhances significantly with the increment in solid volume fraction, resulting in an improvement in the temperature profile as illustrated in Fig. 12. Moreover, it is noteworthy to observe that the influence of solid volume fraction is

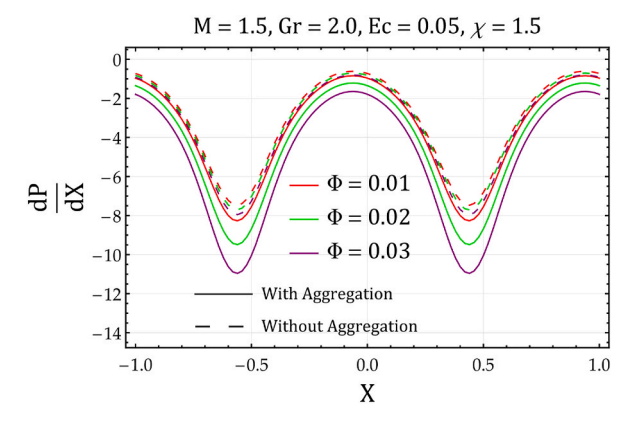


**Fig. 3.** Change of axial pressure gradient  $\frac{dP}{dX}$  with  $\Phi$  (solid volume fraction)..

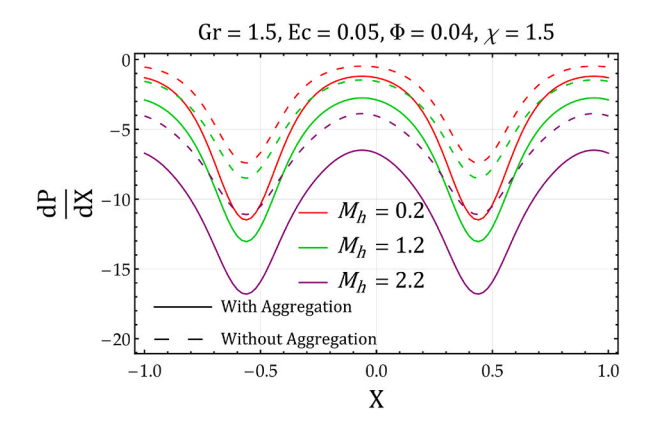
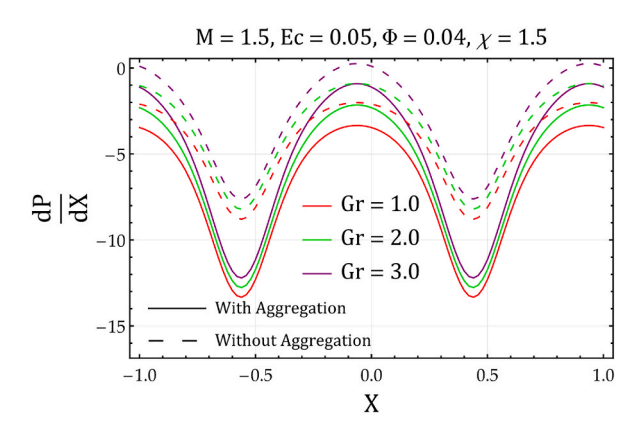


Fig. 4. Change of axial pressure gradient  $\frac{dP}{dX}$  with  $M_h$  (Hartman number).



**Fig. 5.** Change of axial pressure gradient  $\frac{dP}{dX}$  with Gr (Grashof number)..

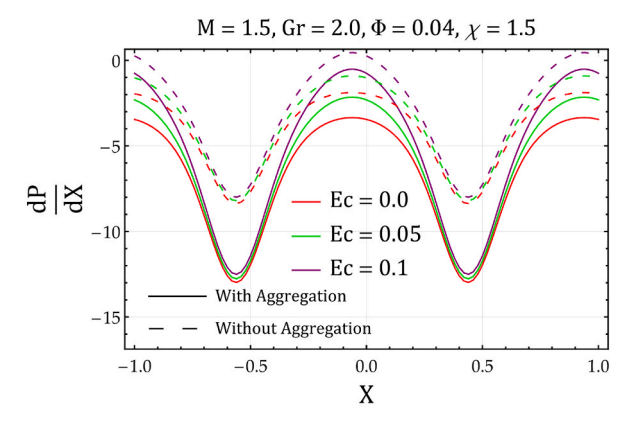


Fig. 6. Change of axial pressure gradient  $\frac{dP}{dX}$  with Ec (Eckert number)..

more conspicuous in nanofluids with NPs aggregation in comparison to those without NPs aggregation.

# 5.5. Temperature profiles

Temperature rise is noticed as the magnetic parameter values increase, as depicted in Fig. 13. Fig. 14 shows temperature profiles boost with a rise in Grashof number. This is because the numerator of the Grashof number includes the term  $\Delta T$  that represents the temperature difference between the two deformable boundaries. Increasing this temperature difference results in a higher Grashof number, which consequently enhances the temperature profile of the nanofluid. The impact on the temperature profile with Eckert number is illustrated in Fig. 15, which demonstrates that a greater Eckert number causes the temperature profile to rise. This behavior is explained by the direct correlation between the transformation of kinetic energy into thermal energy and the Eckert number.

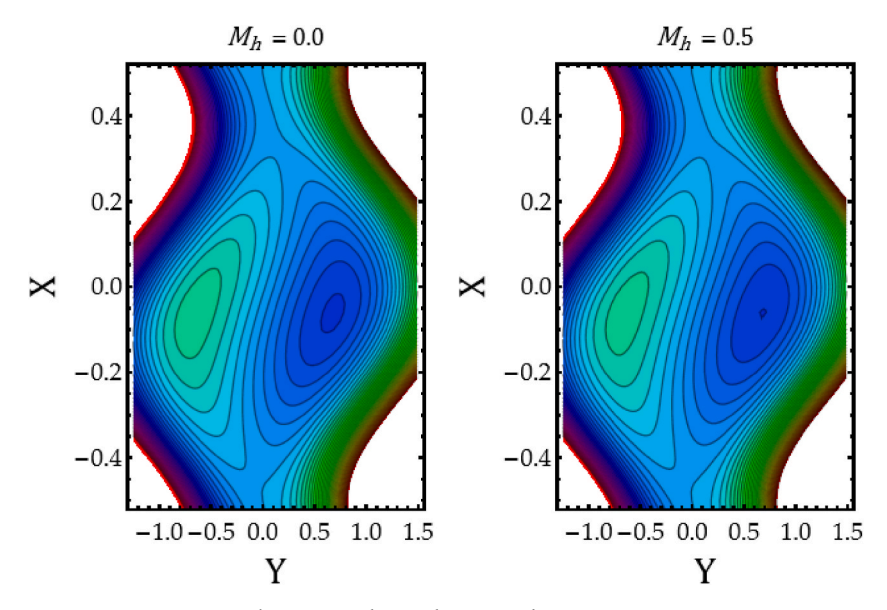


Fig. 7a. Streamlines with nanoparticle aggregation.

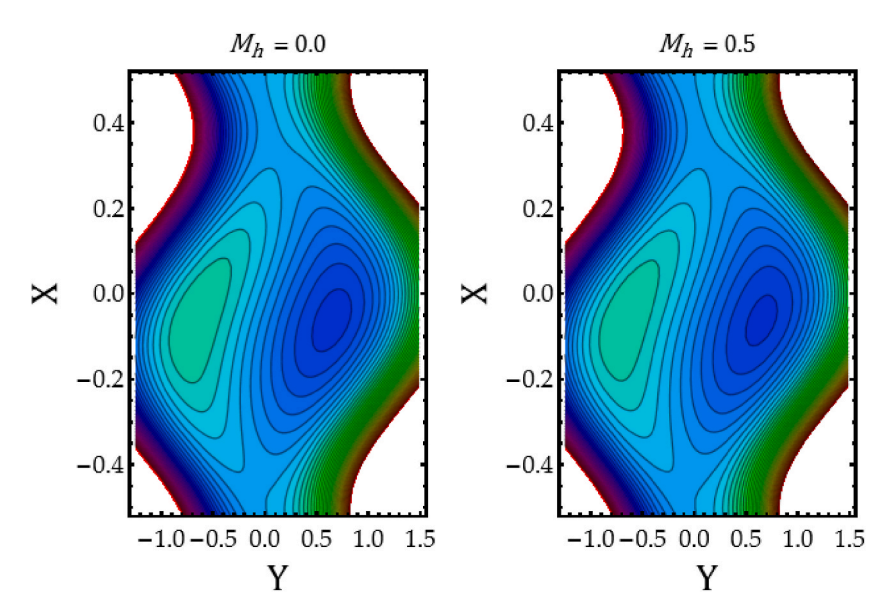


Fig. 7b. Streamlines without nanoparticle aggregation.

# 5.6. Heat transfer rate

(Figs. 16-18) demonstrate the impact of Hartman, Grashof and Eckert number on rate of heat transfer at the right wall of channel respectively. It is noticed that the rate of heat transfer is higher when considering the aggregation of nanoparticles (NPs) as compared to without accounting for this effect. Moreover, the heat transfer rate upsurges with higher values of the magnetic and Eckert numbers but decreases with an increasing Grashof number. The heat transfer rate is further rise with the rise in the solid volume fraction  $\Phi$  of the nanoparticles.

### 5.7. Entropy generation number

Fig. 19 depicts the change in entropy generation Ns across various values of  $\Phi$ . A significant rise in Ns is observed with an increase in  $\Phi$ . Fig. 20 establishes that as the magnetic parameter increases, there is an enhancement in entropy generation, particularly noticeable towards the walls of the channel. This phenomenon can be attributed to the escalation in Joule heating as the magnetic parameters rise, consequently resulting in amplified entropy production. Figs. 21 and 22 respectively show the influence of Grashof and Eckert numbers on entropy generation. It is noticed that entropy generation upsurge with rising values of Eckert and Grashof number. Further, the effects are noticeable close to the deformable walls of the channel. Form Fig. 23, the reduction in entropy

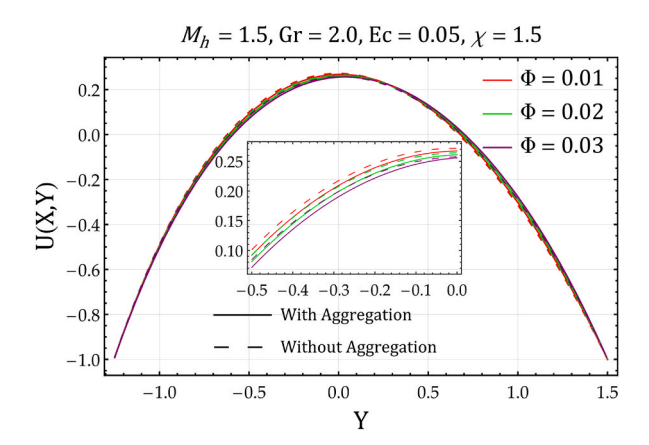


**Fig. 8.** Change of velocity U(X, Y) with  $\Phi$  (solid volume fraction)..

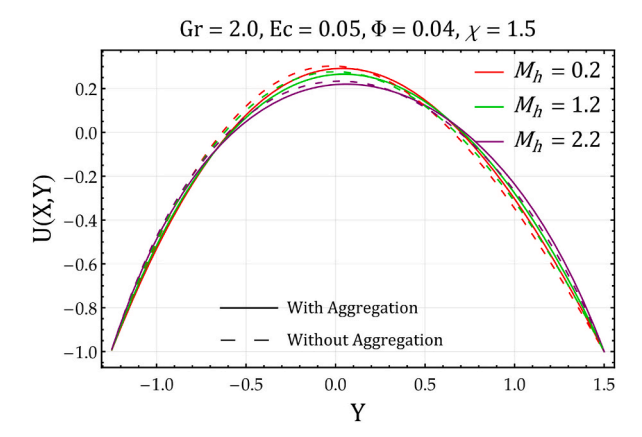


**Fig. 9.** Change of velocity U(X, Y) with  $M_h$  (Hartman number).

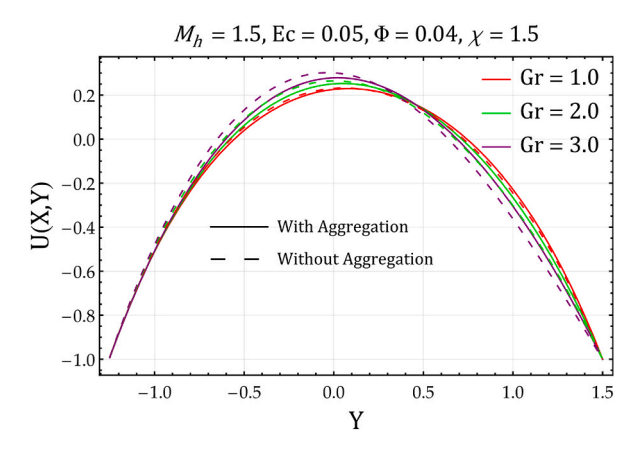
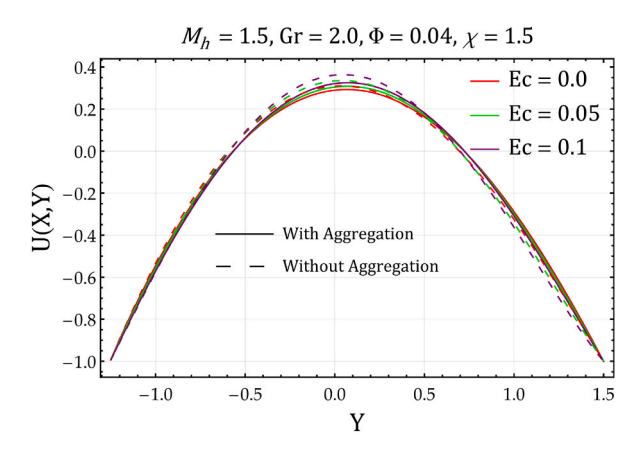


Fig. 10. Change of velocity U(X,Y) with Gr (Grashof number)..

production is noted with growing the temperature difference parameter  $(\theta_d)$  and this is because the denominator of the temperature difference parameter consists of the term  $\Delta T$ , which signifies the temperature difference between the two deformable boundaries. Reducing this temperature difference results in an elevated  $\theta_d$  and, leads to reduce the entropy generation.

# 6. Concluding Remarks

The main findings of this analysis are.



**Fig. 11.** Change of velocity U(X, Y) with Ec (Eckert number)..

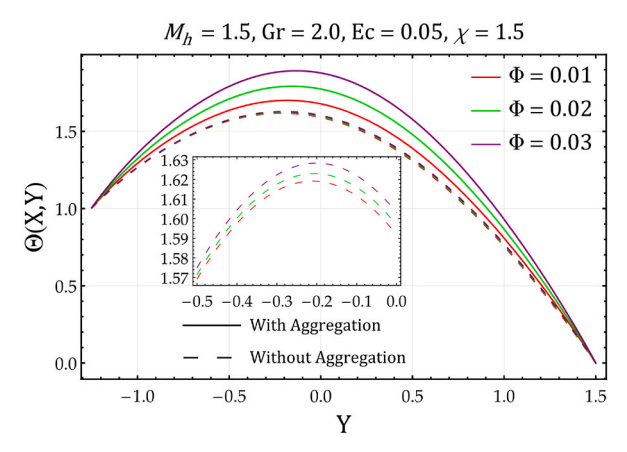


**Fig. 12.** Change of temperature  $\Theta(X,Y)$  with  $\Phi$  (solid volume fraction)..

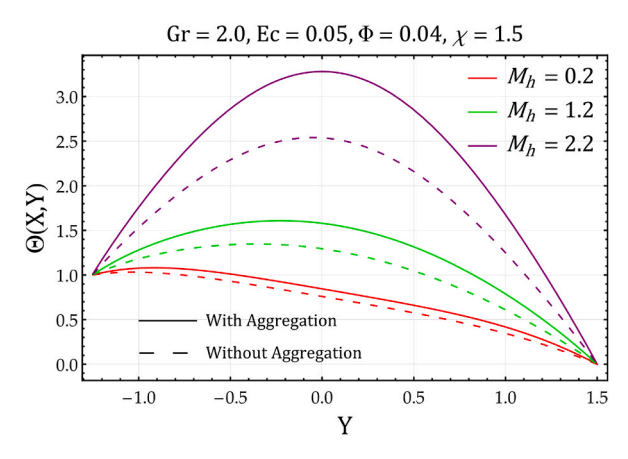
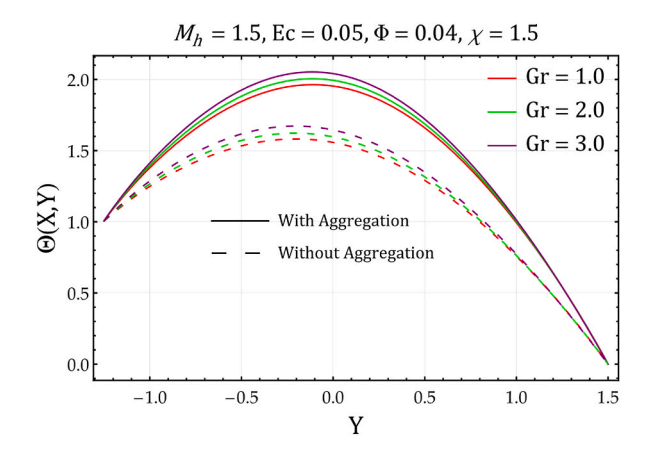
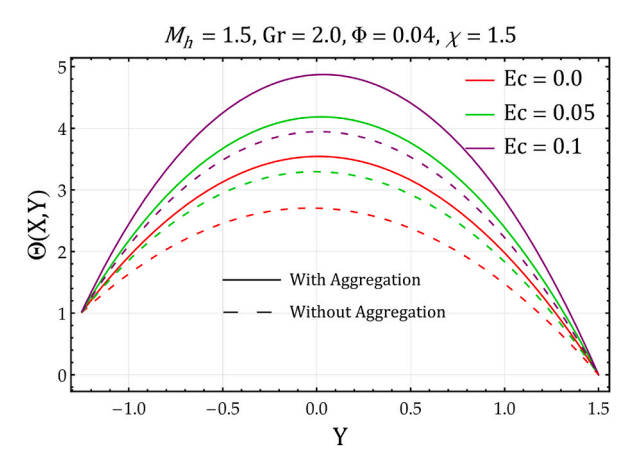


Fig. 13. Change of temperature  $\Theta(X,Y)$  with  $M_h$  (Hartman number).

- Impact of Nanoparticle Aggregation: Nanoparticle aggregation significantly affects the pressure gradient, velocity, heat transfer rate, temperature, and entropy production within the fluid. Aggregation leads to increased viscosity, reduced fluid velocity, and altered thermal and entropy profiles.
- Fluid Trapping: Aggregation results in a reduction in fluid trapping, leading to smaller bolus sizes compared to scenarios without nanoparticle aggregation.



**Fig. 14.** Change of temperature  $\Theta(X, Y)$  with Gr (Grashof number)..



**Fig. 15.** Change of velocity  $\Theta(X, Y)$  with Ec (Eckert number)..

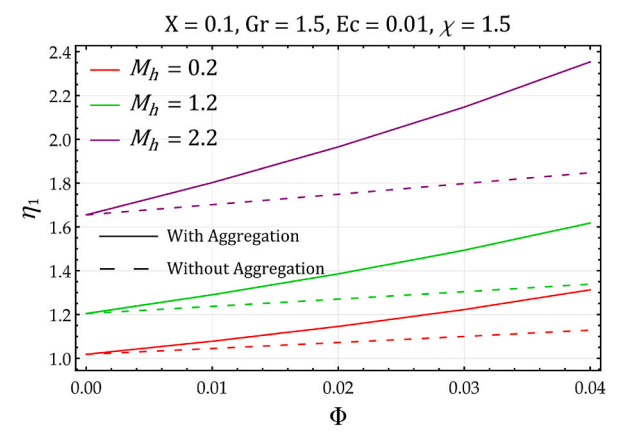


**Fig. 16.** Change of heat transfer rate at  $\eta_1$  (right wall) with  $M_h$  (Hartman number).

- Pressure Gradient: The pressure gradient decreases with rising Grashof and Eckert numbers. However, increased magnetic field strength and higher solid volume fractions of nanoparticles raise the pressure gradient.
- Temperature Profile: Fluid temperature rises with increases in the Grashof number, magnetic parameter, Eckert number, and solid volume fraction of NPs.

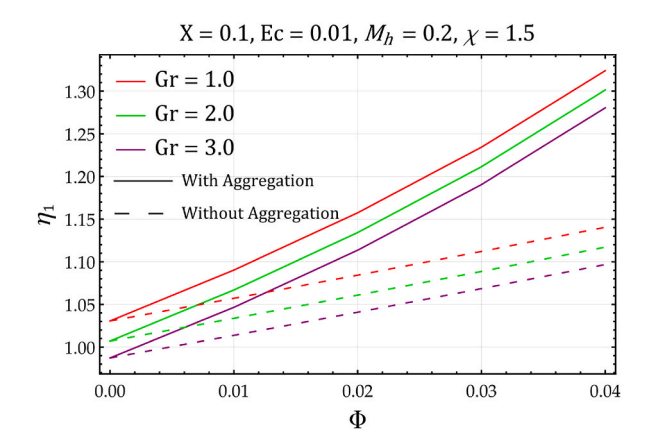


Fig. 17. Change of heat transfer rate at  $\eta_1$  (right wall) with  ${\it Gr}$  (Grashof number)..

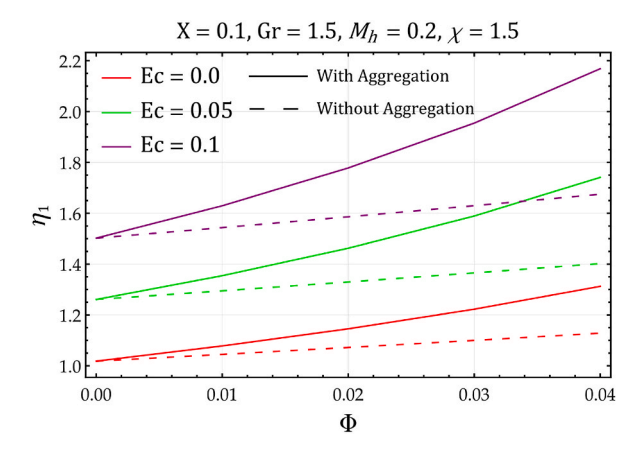


Fig. 18. Change of heat transfer rate at  $\eta_1$  (right wall) with Ec (Eckert number)..

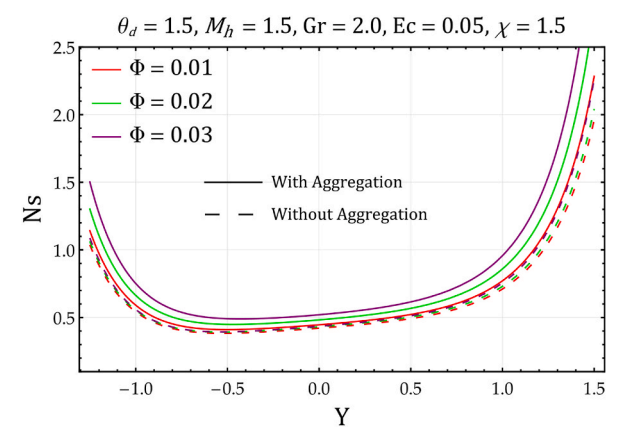


Fig. 19. Change of volumetric entropy generation rate Ns with  $\Phi$  (Solid volume fraction)..

• **Heat Transfer and Entropy Production**: When comparing nanofluids containing aggregated nanoparticles to those without, the former exhibit increased heat transfer rates and entropy generation. Additionally, entropy production can be reduced by decreasing fluid friction and increasing the temperature difference parameter.

# CRediT authorship contribution statement

Muhammad Idrees Afridi: Writing - review & editing, Writing - original draft, Visualization, Validation, Methodology. Abid

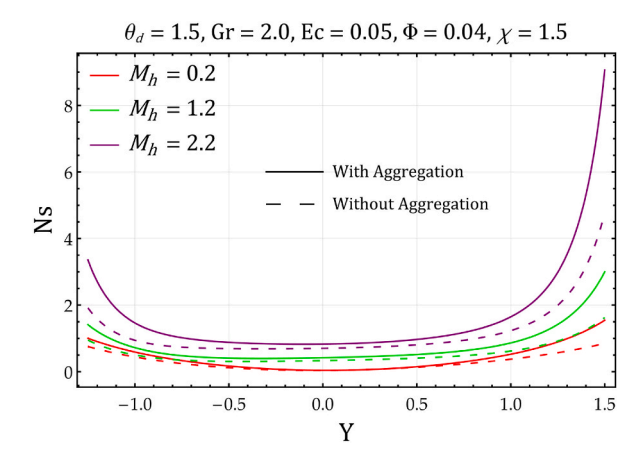


Fig. 20. Change of volumetric entropy generation rate Ns with  $M_h$  (Hartman number).

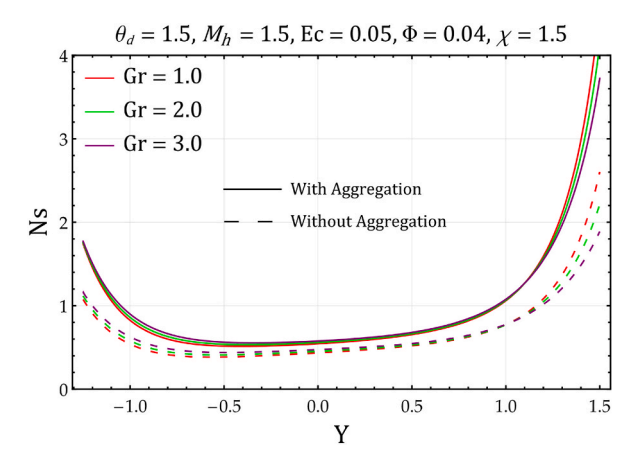


Fig. 21. Change of volumetric entropy generation rate Ns with Gr (Grashof number)..

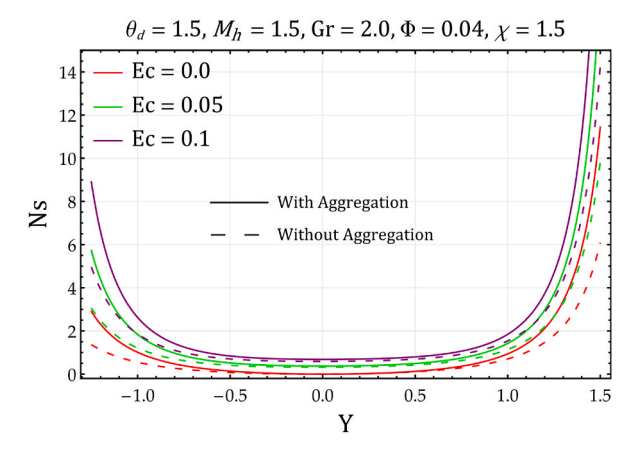


Fig. 22. Change of volumetric entropy generation rate Ns with Ec (Eckert number)..

**Hussanan:** Writing – review & editing, Writing – original draft, Supervision, Formal analysis, Conceptualization. **Muhammad Qasim:** Writing – review & editing, Writing – original draft, Visualization, Supervision, Software. **Ali J. Chamkha:** Writing – review & editing, Writing – original draft, Validation, Supervision, Project administration, Formal analysis, Conceptualization.

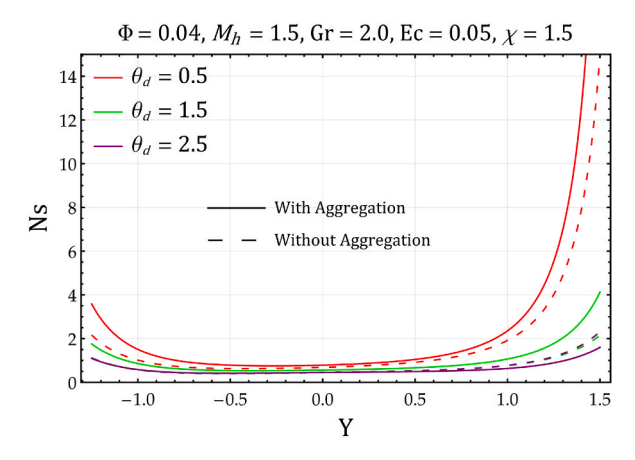


Fig. 23. Change of volumetric entropy generation rate Ns with  $\theta_d$  (Temprature ratio parameter).

# Declaration of competing interest

The authors declare that they have no known competing financial interests or personal relationships that could have appeared to influence the work reported in this paper.

### Data availability

No data was used for the research described in the article.

### Acknowledgement

The first author would like to express his sincere gratitude to Hanjiang Normal University for their generous support and resources that significantly contributed to the completion of this research.

### References

- S.U.S. Choi, Enhancing thermal conductivity of fluids with nanoparticles, The Proceedings of the 1995 ASME International Mechanical Engineering Congress and Exposition 66 (1995) 99–105. San Francisco, USA, ASME, FED 231/MD.
- [2] P.C. Mishra, S. Mukherjee, S.K. Nayak, A. Panda, A brief review on viscosity of nanofluids, Int. Nano Lett. 4 (2014) 109–120.
- [3] S.A. Angayarkanni, John Philip, Review on thermal properties of nanofluids: recent developments, Adv. Colloid Interface Sci. 225 (2015) 146-176.
- [4] W. J. Minkowycz, E M Sparrow and J. P. Abraham, Nanoparticle Heat Transfer and Fluid Flow, CRC Press.
- [5] M. Hatami and D. Jing, Nanofluids: Mathematical, Numerical, and Experimental Analysis, (Academic Press).
- [6] K.R.V. Subramanian, T. N. Rao and A. Balakrishnan, Nanofluids and Their Engineering Applications, CRC Press.
- [7] B. Bhanvase and D. Barai, Nanofluids for Heat and Mass Transfer: Fundamentals, Sustainable Manufacturing and Applications, Academic Press.
- [8] S. K. Das, S.U.S. Choi, W. Yu and T. Pardeep, Nanofluids, Science and Technology, Wiley-Interscience.
- [9] X. Liu, H.I. Mohammed, A.Z. Ashkezari, A. Shahsavar, A.K. Hussein, Sara Rostami, An experimental investigation on the rheological behavior of nanofluids made by suspending multi-walled carbon nanotubes in liquid paraffin, J. Mol. Liq. 300 (2020) 112269.
- [10] S.E. Ahmed, M.A. Mansour, A.K. Hussein, B. Mallikarjuna, M.A. Almeshaal, L. Kolsi, MHD mixed convection in an inclined cavity containing adiabatic obstacle and filled with Cu–water nanofluid in the presence of the heat generation and partial slip, Journal of Thermal Analysis and Calorimetry 138 (2019) 1443–1460.
- [11] B. Ali, S. Hussain, Y. Nie, A.K. Hussein, D. Habib, Finite element investigation of Dufour and Soret impacts on MHD rotating flow of Oldroyd-B nanofluid over a stretching sheet with double diffusion Cattaneo Christov heat flux model, Powder Technol. 377 (2021) 439–452.
- [12] U. Biswal, S. Chakraverty, B.K. Ojha, A.K. Hussein, Numerical investigation on nanofluid flow between two inclined stretchable walls by Optimal Homotopy Analysis Method, Journal of Computational Science 63 (2022) 101759.
- [13] T.W. Latham, Fluid Motion in a Peristaltic Pump, MS, Massachusetts Institute of Technology, Thesis, 1966. Cambridge.
- [14] J.C. Burns, T. Parkes, Peristaltic motion, J. Fluid Mech. 29 (1967) 731-743.
- [15] Y.C. Fung, C.S. Yih, Peristaltic transport, J. Fluid Mech. 35 (1968) 669–675.
- [16] T.F. Zien, S. Ostrach, A long wave approximation to peristaltic motion, J. Biomech. 3 (1970) 63–75.
- [17] A.H. Shapiro, M.Y. Jaffrin, S.L. Weinberg, Peristaltic pumping with long wavelengths at low Reynolds numbers, J. Fluid Mech. 37 (1969) 799–825.
- [18] L.M. Srivastava, V.P. Srivastava, Peristaltic transport: applications to the ducts efferences of the reproductive tract, Rheological Acta 27 (1988) 428-433.
- [19] T.D. Brown, T.K. Hung, Computational and experimental investigations of two-dimensional nonlinear peristaltic flows, J. Fluid Mech. 83 (1977) 249-272.
- [20] N.S. Akbar, Peristaltic Flow of Cu-water nanofluid in a tube, J. Comput. Theor. Nanosci. 11 (2014) 1411–1416.
- [21] S. Noreen, M.M. Rashidi, M. Qasim, Blood flow analysis with considering nanofluid effects in vertical channel, Appl. Nanosci. 7 (2017) 193-199.
- [22] Sara I. Abdelsalam, M.M. Bhatti, The impact of impinging TiO<sub>2</sub> nanoparticles in Prandtl nanofluid along with endoscopic and variable magnetic field effects on peristaltic blood flow, Multidiscip. Model. Mater. Struct. 14 (2018) 530–548.
- [23] J. Prakash, D. Tripathi, O. Anwar Bég, Comparative study of hybrid nanofluids in microchannel slip flow induced by electroosmosis and peristalsis, Appl. Nanosci. 10 (2020) 1693–1706.
- [24] S. Das, B. Barman, R.N. Jana, Influence of hall and Ion-Slip currents on peristaltic transport of magneto-nanofluid in an asymmetric channel, BioNanoScience 11 (2021) 720–738.
- [25] N. Iftikhar, A. Rehman, H. Sadaf, Theoretical investigation for convective heat transfer on Cu/water nanofluid and (SiO<sub>2</sub>-copper)/water hybrid nanofluid with MHD and nanoparticle shape effects comprising relaxation and contraction phenomenon, Int. Commun. Heat Mass Tran. 120 (2021) 105012.
- [26] S. Das, B. Barman, Ramification of hall and Ion-Slip currents on electro-osmosis of ionic hybrid nanofluid in a peristaltic microchannel, BioNanoScience 12 (2022) 957–978.

- [27] M.U. Ashraf, M. Qasim, S. Shafie, Magnetohydrodynamic (MHD) peristaltic flow of blood containing cylindrical shaped gold nanoparticles in a non-uniform tube in the presence of Joule dissipation, J. Magn. Magn Mater. 578 (2023) 170708.
- [28] S. Das, B.N. Barman, R.N. Jana, Hall and ion-slip currents' role in transportation dynamics of ionic Casson hybrid nano-liquid in a microchannel via electroosmosis and peristalsis, Korea-Australia Rheology, Journal 33 (2021) 367–391.
- [29] A. Ali, S. Das, T. Muhammad, Dynamics of blood conveying copper, gold, and titania nanoparticles through the diverging/converging ciliary micro-vessel: further analysis of ternary-hybrid nanofluid, J. Mol. Liq. 390 (2023) 122959.
- [30] S. Waheed, S. Noreen, M. Zahri, A. Soufyane, Electrothermal transport of water conveying copper, silver and alumina nanoparticles through a vertical wavy microchannel, Nanotechnology 34 (2023) 475404.
- [31] A. Ali, F.M. Oudina, A. Barman, S. Das, A.I. Ismail, Peristaltic transportation of hybrid nano-blood through a ciliated micro-vessel subject to heat source and Lorentz force, Journal of Thermal Analysis and Calorimetry 148 (2023) 7059–7083.
- [32] A. Bejan, Entropy Generation through Heat and Fluid Flow, Wiley, New York, 1982.
- [33] A. Bejan, Entropy generation minimization: the new thermodynamics of finite-size devices and finite-time processes, J. Appl. Phys. 79 (1996) 1191-1218.
- [34] O.D. Makinde, A.S. Eegunjobi, Entropy generation in a couple stress fluid flow through a vertical channel filled with saturated porous media, Entropy 15 (2013) 4589–4606.
- [35] A.S. Butt, A. Ali, Entropy analysis of flow and heat transfer caused by a moving plate with thermal radiation, J. Mech. Sci. Technol. 28 (2014) 343-348.
- [36] A.K. Hussein, K. Lioua, R. Chand, S. Sivasankaran, R. Nikbakhti, D. Li, B.M. Naceur, B.A. Habib, Three-dimensional unsteady natural convection and entropy generation in an inclined cubical trapezoidal cavity with an isothermal bottom wall, Alex. Eng. J. 55 (2016) 741–755.
- [37] Abdullah A.A.A. Al-Rashed, W. Aich, L. Kolsi, O. Mahian, A.K. Hussein, M.N. Borjini, Effects of movable-baffle on heat transfer and entropy generation in a cavity saturated by CNT suspensions: three-dimensional modeling, Entropy 19 (2017) 200–216.
- [38] M.I. Afridi, M. Qasim, Entropy generation and heat transfer in boundary layer flow over a thin needle moving in a parallel stream in the presence of nonlinear Rosseland radiation, Int. J. Therm. Sci. 123 (2018) 117–128.
- [39] G.C. Shit, S. Mandal, Entropy analysis on unsteady MHD flow of Casson nanofluid over a stretching vertical plate with thermal radiation effect, International Journal of Applied and Computational Mathematics 6 (2020) 1–22.
- [40] A.A. Alnaqi, A.K. Hussein, L. Kolsi, Abdullah A.A. A. Al-Rashed, D. Li, H.M. Ali, Computational study of natural convection and entropy generation in 3-D cavity with active lateral walls, Therm. Sci. 24 (2020) 2089–2100.
- [41] M.I. Afridi, A. Wakif, M. Qasim, A.J. Chamkha, A generalized differential quadrature approach to the modelling of heat transfer in non-similar flow with nonlinear convection, Int. Commun. Heat Mass Tran. 155 (2024) 107508.
- [42] N.S. Akbar, M. Raza, R. Ellahi, Peristaltic flow with thermal conductivity of H2O + Cu nanofluid and entropy generation, Results Phys. 5 (2015) 115-124.
- [43] M. Qasim, Z.H. Khan, I. Khan, Q.M. Al-Mdallal, Analysis of entropy generation in flow of methanol-based nanofluid in a sinusoidal wavy channel, Entropy 19 (2017) 490.
- [44] N.S. Akbar, A.W. Butt, Entropy generation analysis for the peristaltic flow of Cu-water nanofluid in a tube with viscous dissipation, J. Hydrodyn. 29 (2017) 135–143. Series B.
- [45] S. Noreen, S. Waheed, D.C. Lu, A. Hussanan, Entropy generation in electromagnetohydrodynamic water based three Nano fluids via porous asymmetric microchannel, Eur. J. Mech. B Fluid 85 (2021) 458–466.
- [46] A. Ali, R.N. Jana, S. Das, Significance of entropy generation and heat source: the case of peristaltic blood flow through a ciliated tube conveying Cu-Ag nanoparticles using Phan-Thien-Tanner model, Biomech. Model. Mechanobiol. 20 (2021) 2393–2412.
- [47] R. Ellahi, M. Hassan, A. Zeeshan, Aggregation effects on water base Al<sub>2</sub>O<sub>3</sub>-nanofluid over permeable wedge in mixed convection, Asia Pac. J. Chem. Eng. 11 (2016) 179–186.
- [48] J. Mackolil, B. Mahanthesh, Inclined magnetic field and nanoparticle aggregation effects on thermal Marangoni convection in nanoliquid: a sensitivity analysis, Chin. J. Phys. 69 (2021) 24–37.
- [49] B. Mahanthesh, Flow and heat transport of nanomaterial with quadratic radiative heat flux and aggregation kinematics of nanoparticles, Int. Commun. Heat Mass Tran. 127 (2021) 105521.
- [50] K. Swain, B. Mahanthesh, Thermal enhancement of radiating magneto- nanoliquid with nanoparticles aggregation and Joule heating: a three-dimensional flow, Arabian J. Sci. Eng. 46 (2021) 5865–5873.
- [51] F. Wang, S.P. Rani, K. Sarada, R.J.P. Gowda, U. Khan, H.Y. Zahran, E.E. Mahmoud, The effects of nanoparticle aggregation and radiation on the flow of nanofluid between the gap of a disk and cone, Case Stud. Therm. Eng. 33 (2022) 101930.
- [52] J. Chen, C.Y. Zhao, B.X. Wang, Effect of nanoparticle aggregation on the thermal radiation properties of nanofluids: an experimental and theoretical study, Int. J. Heat Mass Tran. 154 (2020) 11–14.
- [53] H. Chen, Y. Ding, Y. He, C. Tan, Rheological behaviour of ethylene glycol-based titania nanofluids, Chem. Phys. Lett. 444 (2007) 333-337.
- [54] M.K. Nayak, A. Wakif, I.L. Animasaun, M.S.H. Alaoui, Numerical differential quadrature examination of steady mixed convection nanofluid flows over an isothermal thin needle conveying metallic and metallic oxide nanomaterials: a comparative investigation, Arabian J. Sci. Eng. 45 (2020) 5331–5346.
- [55] C. Shu, Differential Quadrature and its Application in Engineering, Springer Science & Business Media, 2012.
- [56] T. Thumma, A. Wakif, I.L. Animasaun, Generalized differential quadrature analysis of unsteady three-dimensional MHD radiating dissipative Casson fluid conveying tiny particles, Heat Transfer 49 (2020) 2595–2626.